

# Strength of the Spin-Fluctuation-Mediated Pairing Interaction in a High-Temperature Superconductor

T. Dahm,<sup>1</sup> V. Hinkov,<sup>2</sup> S. V. Borisenko,<sup>3</sup> A. A. Kordyuk,<sup>3</sup> V. B. Zabolotnyy,<sup>3</sup>  
J. Fink,<sup>3,4</sup> B. Büchner,<sup>3</sup> D. J. Scalapino,<sup>5</sup> W. Hanke,<sup>6</sup> and B. Keimer<sup>2</sup>

<sup>1</sup>*Institute for Theoretical Physics, University of Tübingen, D-72076 Tübingen, Germany*

<sup>2</sup>*Max-Planck-Institute for Solid State Research, D-70569 Stuttgart, Germany*

<sup>3</sup>*IFW Dresden, P.O. Box 270116, D-01171 Dresden, Germany*

<sup>4</sup>*BESSY, D-12489 Berlin, Germany*

<sup>5</sup>*Department of Physics, University of California,  
Santa Barbara, CA 93106-9530, USA*

<sup>6</sup>*Institute for Theoretical Physics, University of Würzburg, D-97074 Würzburg, Germany*

Theories based on the coupling between spin fluctuations and fermionic quasiparticles are among the leading contenders to explain the origin of high-temperature superconductivity, but estimates of the strength of this interaction differ widely [1]. Here we analyze the charge- and spin-excitation spectra determined by angle-resolved photoemission and inelastic neutron scattering, respectively, on the same crystals of the high-temperature superconductor  $\text{YBa}_2\text{Cu}_3\text{O}_{6.6}$ . We show that a self-consistent description of both spectra can be obtained by adjusting a single parameter, the spin-fermion coupling constant. In particular, we find a quantitative link between two spectral features that have been established as universal for the cuprates, namely high-energy spin excitations [2, 3, 4, 5, 6, 7] and “kinks” in the fermionic band dispersions along the nodal direction [8, 9, 10, 11, 12]. The superconducting transition temperature computed with this coupling constant exceeds 150 K, demonstrating that spin fluctuations have sufficient strength to mediate high-temperature superconductivity.

Looking back at conventional superconductors, the most convincing demonstration of the electron-phonon interaction as the source of electron pairing was based on the quantitative correspondence between features in the electronic tunneling conductance and the phonon spectrum measured by inelastic neutron scattering (INS) [13, 14]. The rigorous comparison of fermionic and bosonic spectra was made possible by the Eliashberg theory [15] which allowed one to derive the tunneling conductance from the experimentally determined phonon spectrum. Various difficulties have impeded a similar approach to the origin of high-temperature superconductivity. First, the *d*-wave pairing state found in these materials implies a strongly momentum-dependent pairing interaction. A more elaborate analysis based on data from momentum-resolved experimental techniques such as INS and angle-resolved photoemission spectroscopy (ARPES) is thus required. These methods, in turn, impose conflicting constraints on the materials. In order to avoid surface-related problems, most ARPES experiments have been performed on the electrically neutral BiO

cleavage plane in  $\text{Bi}_2\text{Sr}_2\text{Ca}_{n-1}\text{Cu}_n\text{O}_{2(n+2)+\delta}$  [8]. However, as a consequence of electronic inhomogeneity this family of materials exhibits broad INS spectra that greatly complicate a quantitative comparison with ARPES data [7]. Conversely, compounds with sharp spin excitations, including  $\text{YBa}_2\text{Cu}_3\text{O}_{6+x}$ , have generated problematic ARPES spectra due to polar surfaces with charge distributions different from the bulk [8]. Finally, an analytically rigorous treatment of the spin-fluctuation-mediated pairing interaction is difficult, because small expansion parameters used in the traditional Eliashberg theory (such as the ratio of Debye and Fermi energies) are missing [16]. Because of these difficulties, widely different values have been quoted for the spin-fermion coupling constant [1].

The analysis of  $\text{YBa}_2\text{Cu}_3\text{O}_{6.6}$  data reported here was made possible by recent advances on several fronts. First, INS experiments on this material now consistently yield high-quality spin excitation spectra over a wide energy and momentum range [2, 4]. Second, recent ARPES experiments on  $\text{YBa}_2\text{Cu}_3\text{O}_{6+x}$  [11, 12] have overcome problems related to polar surfaces and allowed the observation of superconducting gaps and band renormalization effects (“kinks”) akin to those previously reported in La- and Bi-based cuprates [8]. Third, calculations based on the two-dimensional (2D) Hubbard model have demonstrated Fermi surfaces, single-particle spectral weights, antiferromagnetic spin correlations, and  $d_{x^2-y^2}$  pairing correlations in qualitative agreement with experimental measurements [17, 18, 19, 20]. Numerically accurate solutions of this model can thus serve as a valuable guideline for a treatment of the spin fluctuation interaction in the cuprates. This is the approach we take here.

Recent quantum Monte Carlo calculations of the 2D Hubbard model within the dynamical cluster approximation (DCA-QMC) [20] have shown that the effective pairing interaction can be parameterized in terms of the numerically computed spin susceptibility  $\chi(\vec{Q}, \Omega)$  in the form

$$V_{eff}(\vec{Q}, \Omega) = \frac{3}{2} \bar{U}^2 \chi(\vec{Q}, \Omega), \quad (1)$$

where  $\bar{U}$  is the coupling strength, and that this interaction generates reasonable values for the superconducting transition temperature  $T_c$ . Here we follow a similar strategy, but

use  $\chi(\vec{Q}, \Omega)$  determined by INS, on high-quality detwinned  $\text{YBa}_2\text{Cu}_3\text{O}_{6.6}$  single crystals described previously [4]. In order to serve as input for the numerical calculations, we have used an analytic form of  $\text{Im}\chi$  that provides an excellent description of the INS data (see the Supplementary Information). Fig. 1 shows a plot of this form in absolute units. In the superconducting state, the spin excitations exhibit the well-known “hour glass” dispersion, with a neck at the wave vector  $\vec{Q} = (\pi, \pi)$  characteristic of antiferromagnetism in the copper oxide planes and the “resonance” energy  $\Omega = 38.5$  meV. (We use a notation in which the lattice parameter  $a$  and the Planck constant  $\hbar$  are set to unity.) The lower branch of the hour glass appears to be influenced by materials-specific details. For instance, recent INS work on  $\text{La}_{2-x}\text{Sr}_x\text{CuO}_4$  indicates two characteristic energies [5, 6], rather than the single resonance found in  $\text{YBa}_2\text{Cu}_3\text{O}_{6+x}$ . The upper branch of high-energy spin excitations, on the other hand, is common to all copper oxides thus far investigated by INS in this energy range [2, 3, 4, 5, 6, 7, 21]. Moreover, while the resonance in  $\text{YBa}_2\text{Cu}_3\text{O}_{6.6}$  disappears above  $T_c$  [4], the intensity of the spin excitations above  $\Omega \sim 50$  meV is not noticeably affected by the superconducting transition and only decreases slowly upon further heating [2, 4].

We extract the second parameter in Eq. 1, the coupling strength  $\bar{U}$ , from a combined analysis of the INS data parameterized in this way and the fermionic band dispersions observed by ARPES on the same crystals (see Methods). As noted before, bonding and antibonding combinations of electronic states on the two Cu-O layers in the  $\text{YBa}_2\text{Cu}_3\text{O}_{6.6}$  unit cell give rise to two distinct Fermi surfaces (Fig. 2). The most prominent signature of many-body effects in the ARPES data, namely the “kink” along the nodal direction (cut #1 in Figs. 3), is highlighted in Fig. 4, where the bonding band is singled out by a proper choice of excitation energy.

We now proceed to a quantitative analysis of the renormalization of the nodal band dispersion by spin fluctuations. Before describing the results, we take a look at the kinematics of spin fluctuation scattering near the nodal points, where complications from the superconducting gap are absent. The spin fluctuations shown in Fig. 1 scatter electrons between bonding and antibonding bands, as indicated by factors in the INS [2, 4] and ARPES

[11, 12] cross sections. (Weak high-energy excitations corresponding to intraband scattering [22] are neglected here.) An analysis of our numerical results below shows that the scattering probability for electrons near the nodal points is greatly enhanced when energy-momentum conservation allows interband scattering into opposite nodal regions (green arrow in Fig. 2). A look at the INS data (green line in Fig. 1) reveals that this condition is satisfied by spin fluctuations of energy  $\sim 80$  meV on the upper, universal, weakly temperature dependent branch of the hour glass. At this characteristic energy in the temperature range studied here, we therefore expect a weakly temperature dependent anomaly in the band dispersion, as experimentally observed.

A self-consistent numerical procedure with a single adjustable parameter, the coupling strength  $\bar{U}$ , was developed to quantitatively assess the influence of the spin-fluctuation interaction on the spectral function determined by ARPES (see the Methods section). Fig. 4 shows that an excellent description of the nodal band dispersion over a wide energy range is obtained with  $\bar{U} = 1.59$  eV, in rough agreement with values found in earlier calculations based on phenomenological models of the spin susceptibility [1]. In particular, both theoretical and experimental results show deviations from linear behavior (“kink”) for  $\omega \geq 80$  meV (arrow in Fig. 4). The corresponding mass renormalization at the nodal point is  $\text{Re } Z_A = 3.7$ .

Fig. 3 shows a comparison of the calculated spectral weight to the ARPES intensity for all three cuts in Fig. 2. It is evident that the calculation yields an excellent description of the ARPES data set over the entire Brillouin zone without further fitting parameters. In particular, the low-intensity region (“dip”) below the renormalized band in cut #3 can be understood as a consequence of coupling to the magnetic resonance at the neck of the hour-glass dispersion. As noted before [1, 23, 24], the resonance wave vector (red lines in Fig. 1 and 2) connects antinodal regions in bonding and antibonding bands, and the resonance and gap energies add up to the dip energy  $\sim 65$  meV. The only noticeable difference between the numerical and experimental data is the width of the momentum distribution curves, which is substantially larger in the ARPES data, presumably at least in part due to residual

surface inhomogeneities [25].

Encouraged by the self-consistent description of INS and ARPES data, we proceed to a calculation of the critical temperature of the  $d$ -wave superconducting state arising from the exchange of spin fluctuations. A recent DCA-QMC study has shown that a good estimate of  $T_c$  can be obtained by using the same effective interaction as in the calculation of the self-energy [20]. For the set of parameters found above, the linearized gap equations (see Methods) yield the  $d$ -wave eigenvalue  $\lambda_d = 1.39$  in the normal state ( $T = 70$  K), corresponding to a transition temperature  $T_c = 174$  K. In principle, the INS and ARPES spectra would now have to be remeasured at this higher temperature, the calculation repeated, etc., until self-consistency is achieved. However, as the spectral weight rearrangement of spin excitations in this temperature range is largely confined to low excitation energies, our estimates for  $\bar{U}$  and  $T_c$  are not expected to change substantially (see Methods). In this context it is instructive to compare the eigenvalue at  $T = 70$  K with the one obtained from the INS spectrum at 5 K that includes the “resonance”,  $\lambda_d = 1.49$ . The enhanced eigenvalue implies that the redistribution of spectral weight of the spin excitations below  $T_c$  leads to an increase of the effective pairing strength. This lends support to an interpretation of the magnetic resonance and associated antinodal dip in terms of a superconductivity-induced feedback effect on the spin fluctuation spectrum [1]. It is also consistent with the large  $2\Delta_0/k_B T_c$  ratio.

In summary, we have shown that data from two momentum-resolved experimental probes of a cuprate superconductor can be related in a quantitative fashion, in close analogy to the traditional analysis of the electron-phonon interaction in conventional superconductors. Our analysis is in overall agreement with conclusions drawn from prior work based on phenomenological spin excitation spectra and/or data from probes without momentum resolution [1, 23, 24, 26, 27, 28], and it resolves some problems that appeared in the context of these studies. In particular, models that attribute the nodal kink in ARPES either directly to the magnetic resonance [23, 29] or to incoherent scattering processes from a node into gapped states at the antinode [24] generally predict that the kink is strongly modified by the

onset of superconductivity, whereas the experiments indicate at most a weak effect at  $T_c$  [10]. The node-to-node interband scattering process mediated by weakly temperature dependent, universal, incommensurate spin excitations we have identified provides a straightforward explanation of this observation. As the incommensurate spin excitations persist into the optimally doped [5, 7] and overdoped [6] regimes, it also explains the persistence of both the kink and superconductivity at high doping, where feedback effects related to the magnetic resonance are progressively reduced [27]. There is thus no need to invoke phonon scattering at this level [9]. While some contribution of phonons to the nodal kink cannot be ruled out, recent work has shown that it is hard to obtain a quantitative description of the kink based on the electron-phonon interaction alone [24, 30, 31].

It was previously shown [32] that the change in the magnetic exchange energy between the normal and superconducting states is more than enough to account for the cuprate superconducting condensation energy. However, the crucial question whether the exchange of magnetic spin-fluctuations actually has the strength to give rise to high- $T_c$  pairing, was not answered. Here we have shown that this interaction can generate  $d$ -wave superconducting states with transition temperatures comparable to the maximum  $T_c$  observed in the cuprates. In any given material, especially underdoped cuprates such as  $\text{YBa}_2\text{Cu}_3\text{O}_{6.6}$ , a variety of effects not considered in our analysis can reduce the actual  $T_c$ , including vertex corrections of the spin fluctuation interaction [16], phase fluctuations of the order parameter, competition with other types of order, and pair breaking by phonons and impurities. It is also possible that phonons [9, 30, 31] or higher-energy excitations [33] contribute to the pairing interaction. However, our analysis indicates that the exchange of spin excitations already directly observed by INS is a major factor driving the high temperature superconducting state in the cuprates.

## Methods

The ARPES measurements were performed on the same  $\text{YBa}_2\text{Cu}_3\text{O}_{6.6}$  crystals used for the INS experiment, thus avoiding systematic uncertainties invariably associated with measurements on different materials. The details of the ARPES experiments have been described elsewhere [11, 12]. Usually, YBCO single crystals cleave between the Ba-O and Cu-O chain layers, resulting in an effective overdoping of the Cu-O layer closest to the surface [11, 12, 34]. A recent comprehensive study has revealed, however, that in some cases the ARPES spectra are dominated by a signal from the nominally doped Cu-O plane [12]. Here we present data taken on a particular spot on the surface after one such successful cleave (Figs. 2, 3). The strong many-body renormalization of the band structure typical for underdoped cuprates (Fig. 4) as well as the anisotropic superconducting gap (cuts #2, 3 in Fig. 3) in the ARPES spectra demonstrate that contributions from the overdoped surface-related component are negligible. The superconducting component we observe corresponds to the nominal doping, as follows from the size of the gap and the temperature evolution of the coherence peaks which disappear above the bulk SC transition temperature [12].

The self-consistent numerical calculation we have used is based on the self-energy diagram displayed in Fig. 4. The Green's functions  $G(\vec{k}, \omega)$  on antibonding ( $A$ ) and bonding ( $B$ ) bands can be written as [18]

$$G_{A,B}(\vec{k}, \omega) = \frac{\omega Z_{A,B} + \tilde{\epsilon}_k^{A,B}}{(\omega Z_{A,B})^2 - (\tilde{\epsilon}_k^{A,B})^2 - (\text{Re } Z_{A,B}(\vec{k}, \omega = 0) \Delta_k)^2} \quad (2)$$

where  $\Delta_k$  is the superconducting gap, which we assume to be of the  $d$ -wave form  $\Delta_k = \Delta_0(\cos k_x - \cos k_y)/2$  with  $\Delta_0 = 30$  meV, and  $\tilde{\epsilon}_k^{A,B} = \epsilon_k^{A,B} + \xi_{A,B}$  is the renormalized band structure. The unrenormalized band dispersions  $\epsilon_k^{A,B}$  were derived from tight-binding fits to the ARPES Fermi surface in combination with additional information from band structure calculations (see the Supplementary Information). We have found that the results of our calculations are quite robust against modifications of  $\epsilon_k^{A,B}$  (see the Supplementary Information). Finally,  $\omega Z_{A,B}(\vec{k}, \omega) = \omega - \frac{1}{2} (\Sigma_{A,B}(\vec{k}, \omega) - \Sigma_{A,B}^*(\vec{k}, -\omega)) + i\Gamma_{el}$  is the mass renormalization function and  $\xi_{A,B}(\vec{k}, \omega) = \frac{1}{2} (\Sigma_{A,B}(\vec{k}, \omega) + \Sigma_{A,B}^*(\vec{k}, -\omega))$  the energy shift

function. Apart from an elastic scattering rate  $\Gamma_{el} \sim 30$  meV, which accounts for impurity scattering, the mass renormalization function is determined by the imaginary part of the electron self-energy  $\Sigma_{A,B}$ , which can be written as

$$\text{Im } \Sigma_{A,B}(\vec{k}, \omega) = \frac{1}{\pi N} \sum_Q \int_{-\infty}^{\infty} d\Omega [n(\Omega) + f(\Omega - \omega)] \text{Im } V_{eff}(\vec{Q}, \Omega) \text{Im } G_{B,A}(\vec{k} - \vec{Q}, \omega - \Omega). \quad (3)$$

Here  $\sum_Q$  denotes a sum of the in-plane momenta over the full Brillouin zone,  $n$  and  $f$  are the Bose- and Fermi-functions, respectively, and  $V_{eff}$  is the spin fluctuation interaction (Eq. 1). The real parts of  $\Sigma_{A,B}$  that enter into Eq. 2 are obtained by Kramers-Kronig transformations. Note that the self-energy in the antibonding band is determined by the interaction with the bonding band and vice versa.

Together with Eq. 1, this defines a self-consistent system of equations with a single adjustable parameter, the coupling strength  $\bar{U}$ . Starting with noninteracting values for the Green's functions, these equations were solved iteratively until convergence is achieved. The renormalized band dispersion and spectral weight,  $f(\omega) \text{Im } G(\vec{k}, \omega)$ , can then be compared to ARPES data.

The linearized gap equations

$$\lambda_d \text{Im } \phi_{A,B}(\vec{k}, \omega) = \frac{1}{\pi N} \sum_{k'} \int_{-\infty}^{\infty} d\omega' [n(\omega - \omega') + f(-\omega')] \text{Im } V_{eff}(\vec{k} - \vec{k}', \omega - \omega') \text{Im } \left\{ \frac{\phi_{B,A}(\vec{k}', \omega')}{(\omega' Z_{B,A})^2 - (\tilde{\epsilon}_{k'}^{B,A})^2} \right\} \quad (4)$$

were solved for the same set of parameters. Note that the INS data used for the calculations were taken at  $T = 5$  and 70 K, while the ARPES data were taken at 30 K. Since the changes in the superconducting gap and INS spectrum between 5 and 30 K are negligible, we use the 5 K INS results along with the 30 K ARPES data to determine the coupling constant  $\bar{U}$ . As  $T$  is raised further, the superconducting gap decreases, and there is a shift of  $\text{Im}\chi$  to lower frequencies. However, we expect that  $\bar{U}$  is unchanged for the range of temperatures of interest, because it is determined by weakly  $T$ -dependent high-energy processes.

For discussions of the influence of a high-energy cutoff in  $\chi(\vec{Q}, \Omega)$  and of a normal-state

pseudogap on the results of the numerical calculations, see the Supplementary Information.

---

- [1] Eschrig, M. The effect of collective spin-1 excitations on electronic spectra in high- $T_c$  superconductors. *Adv. Phys.* **55**, 47 (2006).
- [2] Hayden, S. M., Mook, H. A., Dai, P., Perring, T. G. & Dogan, F. The structure of the high-energy spin excitations in a high-transition-temperature superconductor. *Nature* **429**, 531 (2004).
- [3] Tranquada, J. M. *et al.* Quantum magnetic excitations from stripes in copper oxide superconductors. *Nature* **429**, 534 (2004).
- [4] Hinkov, V. *et al.* Spin dynamics in the pseudogap state of a high-temperature superconductor. *Nat. Phys.* **3**, 780 (2007).
- [5] Vignolle, B. *et al.* Two energy scales in the spin excitations of the high-temperature superconductor  $\text{La}_{2-x}\text{Sr}_x\text{CuO}_4$ . *Nat. Phys.* **3**, 163–167 (2007).
- [6] Lipscombe, O. J., Hayden, S. M., Vignolle, B., McMorrow, D. F. & Perring, T. G. Persistence of high-frequency spin fluctuations in overdoped superconducting  $\text{La}_{2-x}\text{Sr}_x\text{CuO}_4$  ( $x = 0.22$ ). *Phys. Rev. Lett.* **99**, 067002 (2007).
- [7] Fauqué, B. *et al.* Dispersion of the odd magnetic resonant mode in nearly-optimally doped  $\text{Bi}_2\text{Sr}_2\text{CaCu}_2\text{O}_{8+\delta}$ . *Phys. Rev. B* **76**, 214512 (2007).
- [8] Damascelli, A., Hussain, Z. & Shen, Z.-X. Angle-resolved photoemission studies of the cuprate superconductors. *Rev. Mod. Phys.* **75**, 473–541 (2003).
- [9] Lanzara, A. *et al.* Evidence for ubiquitous strong electron-phonon coupling in high-temperature superconductors. *Nature* **412**, 510–514 (2001).
- [10] Kordyuk, A. A. *et al.* Constituents of the quasiparticle spectrum along the nodal direction of high- $T_c$  cuprates. *Phys. Rev. Lett.* **97**, 017002 (2006).
- [11] Borisenko, S. V. *et al.* Kinks, nodal bilayer splitting and interband scattering in  $\text{YBa}_2\text{Cu}_3\text{O}_{6+x}$ . *Phys. Rev. Lett.* **96**, 117004 (2006).
- [12] Zabolotnyy, V. B. *et al.* Momentum and temperature dependence of renormalization effects in the high-temperature superconductor  $\text{YBa}_2\text{Cu}_3\text{O}_{7-\delta}$ . *Phys. Rev. B* **76**, 064519 (2007).
- [13] McMillan, W. L. & Rowell, J. M. Lead phonon spectrum calculated from superconducting density of states. *Phys. Rev. Lett.* **14**, 108 (1965).

- [14] For a review, see the articles by D. J. Scalapino and W. L. McMillan and J. M. Rowell in *Superconductivity* Vol. 1, ed. R. D. Parks (Marcel Dekker, New York, 1969).
- [15] Eliashberg, G. M. *Sov. Phys. JETP* **11**, 696 (1960).
- [16] Huang, Z. B., Hanke, W., Arrigoni, E. & Chubukov, A. V. Renormalization of the electron-spin-fluctuation interaction in the  $t$ - $t'$ - $U$  Hubbard model. *Phys. Rev. B* **74**, 184508 (2006).
- [17] S en echal, D., Lavertu, P.-L., Marois, M.-A. & Tremblay, A.-M. S. Competition between antiferromagnetism and superconductivity in high- $T_c$  cuprates. *Phys. Rev. Lett.* **94**, 156404 (2005).
- [18] Dahm, T. & Tewordt, L. Physical quantities in nearly antiferromagnetic and superconducting states of the two-dimensional Hubbard model and comparison with cuprate superconductors. *Phys. Rev. B* **52**, 1297 (1995).
- [19] Aichhorn, M., Arrigoni, E., Potthoff, M. & Hanke, W. Phase separation and competition of superconductivity and magnetism in the two-dimensional Hubbard model: From strong to weak coupling. *Phys. Rev. B* **76**, 224509 (2007).
- [20] Maier, T. A., Macridin, A., Jarrell, M. & Scalapino, D. J. Systematic analysis of a spin-susceptibility representation of the pairing interaction in the two-dimensional Hubbard model. *Phys. Rev. B* **76**, 144516 (2007).
- [21] Bourges, P. *et al.* The spin excitations spectrum in superconducting  $\text{YBa}_2\text{Cu}_3\text{O}_{6.85}$ . *Science* **288**, 1234–1237 (2000).
- [22] Pailh es, S. *et al.* Doping dependence of bilayer resonant spin excitations in  $(\text{Y,Ca})\text{Ba}_2\text{Cu}_3\text{O}_{6+x}$ . *Phys. Rev. Lett.* **96**, 257001 (2006).
- [23] Eschrig, M. & Norman, M. R. Effect of the magnetic resonance on the electronic spectra of high- $T_c$  superconductors. *Phys. Rev. B* **67**, 144503 (2003).
- [24] Chubukov, A. V. & Norman, M. R. Dispersion anomalies in cuprate superconductors. *Phys. Rev. B* **70**, 174505 (2004).
- [25] Graser, S., Hirschfeld, P. J. & Scalapino, D. J. Local quasiparticle lifetimes in a  $d$ -wave superconductor. *Phys. Rev. B* **77**, 184504 (2008).
- [26] Carbotte, J. P., Schachinger, E. & Basov, D. N. Coupling strength of charge carriers to spin fluctuations in high-temperature superconductors. *Nature* **401**, 354–356 (1999).
- [27] Hwang, J., Timusk, T. & Gu, G. D. High-transition-temperature superconductivity in the absence of the magnetic-resonance mode. *Nature* **427**, 714–717 (2004).

- [28] Hwang, J. *et al.* Bosonic spectral density of epitaxial thin-film  $\text{La}_{1.83}\text{Sr}_{0.17}\text{CuO}_4$ . *Phys. Rev. Lett.* **100**, 137005 (2008).
- [29] Manske, D., Eremin, I. & Bennemann, K. H. Renormalization of the elementary excitations in hole- and electron-doped cuprates due to spin fluctuations. *Phys. Rev. B* **67**, 134520 (2003).
- [30] Giustino, F., Cohen, M. L. & Louie, S. G. Small phonon contribution to the photoemission kink in the copper oxide superconductors. *Nature* **452**, 975–978 (2008).
- [31] Heid, R., Bohnen, K.-P., Zeyher, R. & Manske, D. Momentum dependence of the electron-phonon coupling and self-energy effects in superconducting  $\text{YBa}_2\text{Cu}_3\text{O}_7$  within the local density approximation. *Phys. Rev. Lett.* **100**, 137001 (2008).
- [32] Woo, H. *et al.* Magnetic energy change available to superconducting condensation in optimally doped  $\text{YBa}_2\text{Cu}_3\text{O}_{6.95}$ . *Nat. Phys.* **2**, 600–604 (2006).
- [33] Pasupathy, A. N. *et al.* Electronic origin of the inhomogeneous pairing interaction in the high- $T_c$  superconductor  $\text{Bi}_2\text{Sr}_2\text{CaCu}_2\text{O}_{8+\delta}$ . *Science* **320**, 196–201 (2008).
- [34] Hossain, M. *et al.* In situ doping control of the surface of high-temperature superconductors. *Nat. Phys.* **4**, 527–531 (2008).

**Acknowledgements.** This project is part of the Forschergruppe FOR538 of the German Research Foundation. DJS acknowledges the Center for Nanophase Material Sciences at Oak Ridge National Laboratory, U.S. Department of Energy. We thank P. Bourges and A. Ivanov for discussions.

Correspondence and requests for materials should be addressed to B.K. (b.keimer@fkf.mpg.de).

Supplementary Information accompanies this paper on [www.nature.com/naturephysics](http://www.nature.com/naturephysics).

**Competing financial interests.** The authors declare that they have no competing financial interests.

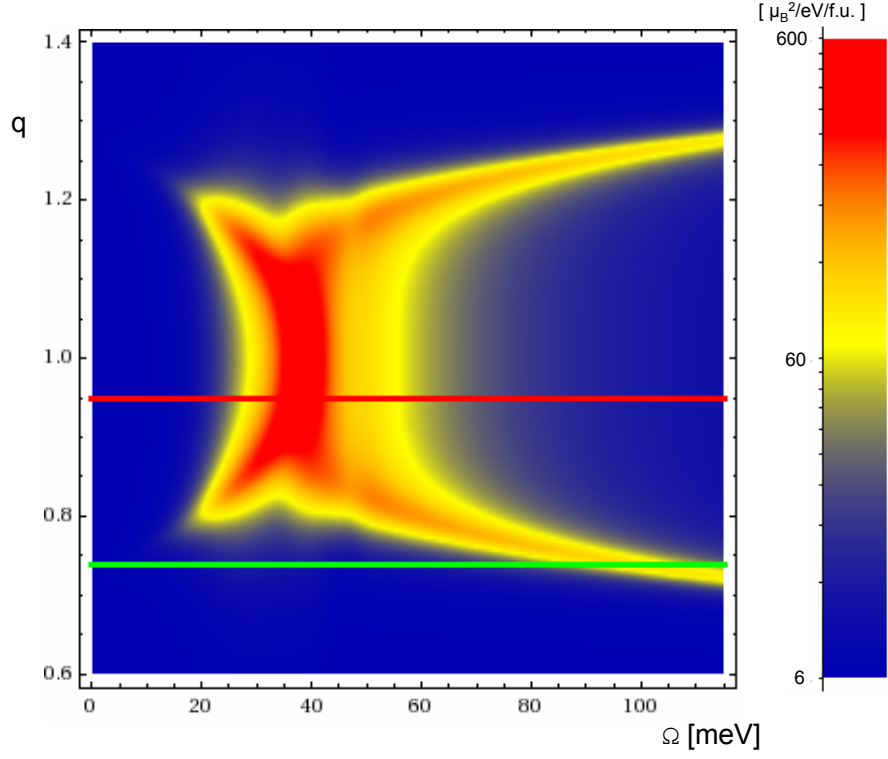


FIG. 1: Intensity of spin excitations along  $\vec{Q} = q(\pi, \pi)$  resulting from numerical fits to the INS spectra of  $\text{YBa}_2\text{Cu}_3\text{O}_{6.6}$  at  $T = 5$  K. The maximum value corresponds to  $600 \mu_B^2/\text{eV}/\text{f.u.}$  The green (red) lines mark wave vectors connecting nodal (antinodal) regions on different Fermi surfaces (Fig. 2).

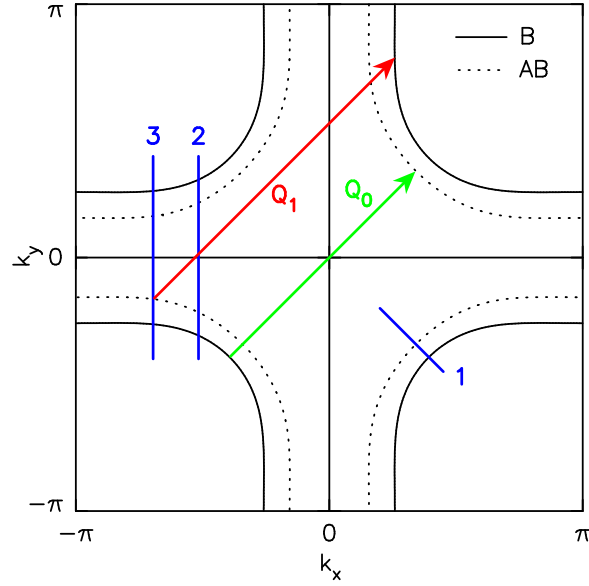


FIG. 2: Results of tight-binding fits of the Fermi surfaces determined by ARPES for the bonding (solid line) and antibonding (dotted line) bands. The blue lines denote the three cuts along which experimental and theoretical spectral functions are compared (Fig. 3). The green and red arrows indicates spin-fluctuation-mediated scattering processes discussed in the text.

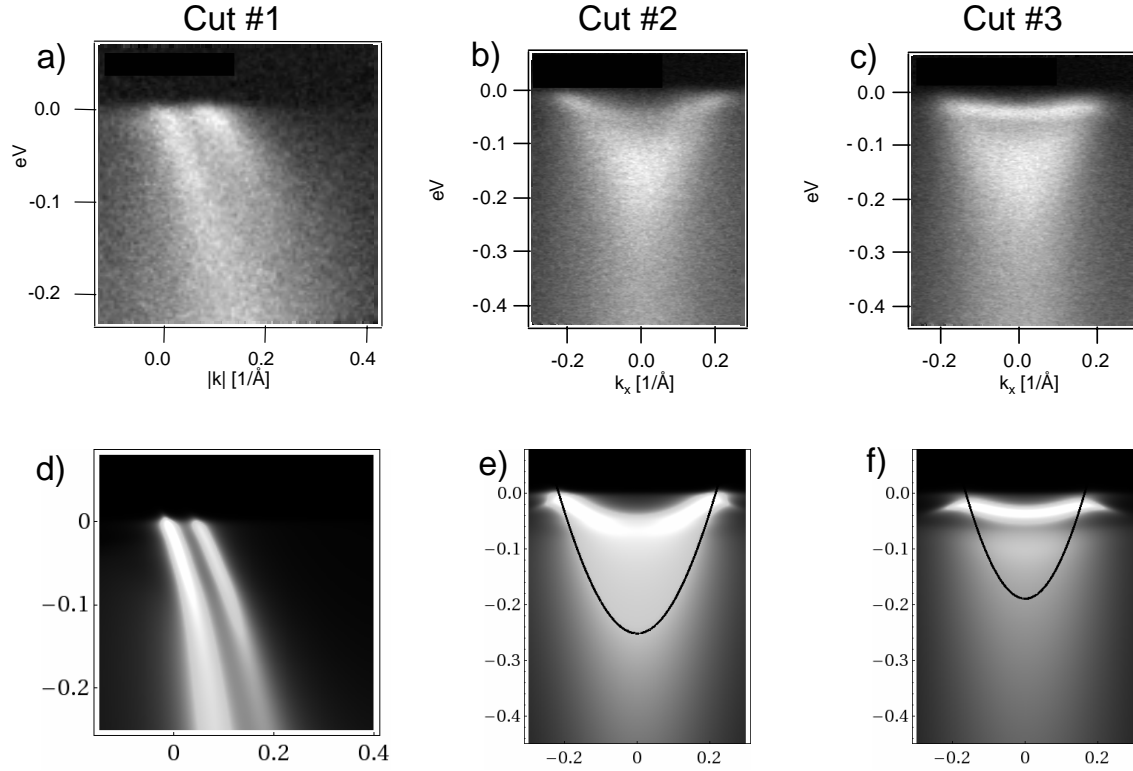


FIG. 3: **a–c** ARPES intensities at 30 K along the three cuts shown in Fig. 2, obtained with photon energies 60 eV (cut #1) and 55 eV (cuts #2, 3). **d–f** Theoretical spectral functions at  $T = 5$  K, multiplied by the Fermi function at 30 K (see Methods). Intensities in bonding and antibonding bands in panel **d** were multiplied by 0.75 and 0.25, respectively, to take account of matrix element effects. The black lines in panels **e** and **f** show the unrenormalized antibonding band dispersion.

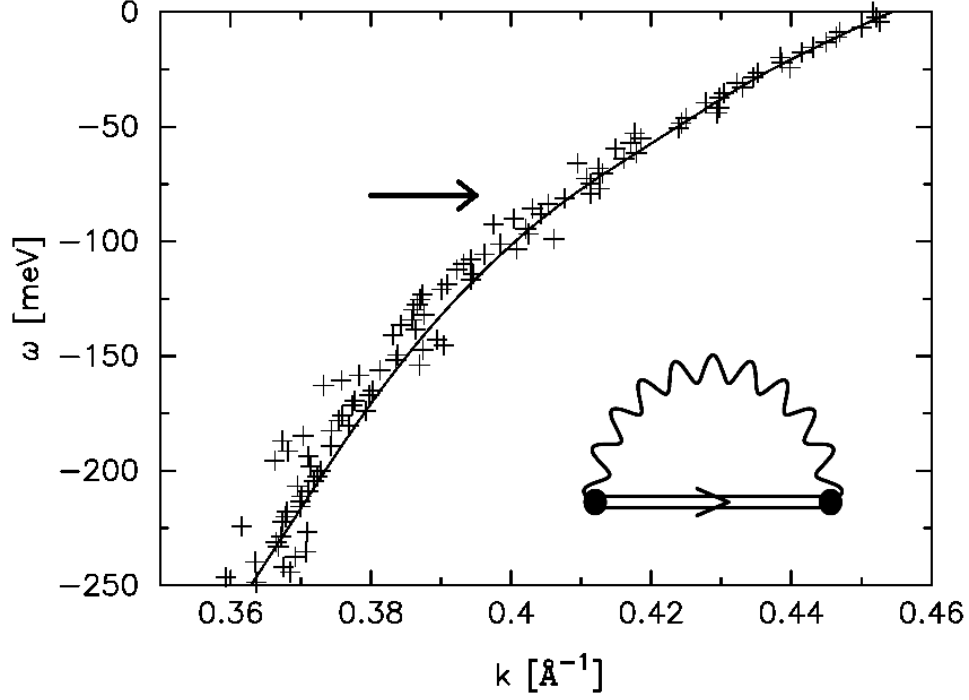


FIG. 4: Nodal dispersion of the ARPES data (crosses) for the bonding band compared with the same nodal dispersion of the calculation (solid line). Here, the coupling constant  $\bar{U}$  was adjusted such that the slopes of the curves (renormalized Fermi velocity) match near zero energy. The inset shows a self-energy diagram for the exchange of spin fluctuations. The wiggly line represents the interaction given by Eq. 1, and the straight double line is the self-consistent single-particle Green's function.

**Supplementary Information for “Strength of the  
Spin-Fluctuation-Mediated Pairing Interaction in a  
High-Temperature Superconductor”**

## Fit to INS data

The INS results were fitted by simple analytic forms which could then be numerically integrated in the self-energy and  $T_c$  calculations. In constructing these fits, the energy range was divided into upper ( $u$ ) and lower ( $\ell$ ) branches corresponding to energies above and below the resonance energy  $\omega_r$ .

$$\text{Im } \chi(\vec{Q}, \Omega) = \text{Im } \chi_\ell(\vec{Q}, \Omega) + \text{Im } \chi_u(\vec{Q}, \Omega) \quad (5)$$

The data in the superconducting state at  $T = 5$  K were fitted as follows. On the lower branch

$$\text{Im } \chi_\ell(\vec{Q}, \Omega) = N_0 N_\ell(\Omega) N_L(\Omega) \frac{2(2\Omega_r - \Omega)\gamma_Q}{((2\Omega_r - \Omega)^2 - \Omega_Q^2)^2 + (2(2\Omega_r - \Omega)\gamma_Q)^2} \quad (6)$$

Here the frequency  $\Omega$  is measured in meV with the resonance frequency  $\Omega_r = 38.5$  meV.

The prefactors are given by

$$N_\ell(\Omega) = 1 - \frac{1}{1 + \exp[(\Omega - 24)/3]} \quad (7)$$

and

$$N_L(\Omega) = \frac{1}{1 + \exp[\Omega - 42]} \quad (8)$$

These factors essentially cut off the lower branch at frequencies above 42 meV and below 24 meV (spin gap). The momentum dispersion of the resonance mode is given by

$$\Omega_Q = \Omega_r + s_a(Q_a - Q_{0a})^2 + s_b(Q_b - Q_{0b})^2 \quad (9)$$

with  $\mathbf{Q}_0 = (Q_{0a}, Q_{0b})$  the antiferromagnetic wave vector,  $s_a = 280$  meV  $\text{\AA}^2$  and  $s_b = 455$  meV  $\text{\AA}^2$ . The damping width  $\gamma_Q$  has an angular dependence of the form

$$\gamma_Q = \gamma_a + \Delta\gamma \frac{(Q_a - Q_{0a})^2}{|\mathbf{Q} - \mathbf{Q}_0|^2} \quad (10)$$

where the index  $a$  denotes the  $a$ -axis direction in the Brillouin zone and  $b$  the  $b$ -axis direction, respectively. The parameter values are  $\gamma_a = 1.5$  meV and  $\Delta\gamma = 6.5$  meV.

For the upper branch we have

$$\text{Im } \chi_u(\vec{Q}, \Omega) = N_0 N_{0u} N_u(\Omega) N_{dip}(\Omega) N_{rot}(\vec{Q}) \frac{2\Omega\Gamma}{(\Omega^2 - \Omega_Q^2)^2 + (2\Omega\Gamma)^2} \quad (11)$$

Here,  $\Gamma = 11$  meV and

$$\Omega_Q = \Omega_r + \left[ S_a^{2/p} (Q_a - Q_{0a})^2 + S_b^{2/p} (Q_b - Q_{0b})^2 \right]^{p/2} \quad (12)$$

where  $p = 4$  is the power of the dispersion of the upper branch (somewhat steeper than quadratic) with  $S_a = 4830$  meV  $\text{\AA}^p$  and  $S_b = 10065$  meV  $\text{\AA}^p$ . The prefactor  $N_{0u}$  is 1.35 and

$$N_u(\Omega) = 1 - \frac{1}{1 + \exp[(\Omega - 36)/1.5]} \quad (13)$$

provides a cut-off of the upper branch for energies below 36 meV. The prefactor

$$N_{dip}(\Omega) = 1 - 0.2 \exp \left[ -(\Omega - \Omega_{dip})^2 / (2\sigma_{dip}^2) \right] \quad (14)$$

with  $\Omega_{dip} = 47$  meV and  $\sigma_{dip} = 2$  meV accounts for the reduction in intensity just above the resonance. The prefactor  $N_{rot}$  has a momentum dependence of the form

$$N_{rot}(\vec{Q}) = 1 - 0.3 \left( \frac{((Q_a - Q_{0a})^2 - (Q_b - Q_{0b})^2)^2}{|\mathbf{Q} - \mathbf{Q}_0|^2} \right)^2 \quad (15)$$

accounting for the 45 degree rotation of the signal above the resonance [S1, S2]. The overall normalization factor  $N_0$  is chosen such that the momentum integrated  $\text{Im } \chi(\vec{q}, \Omega)$  has a peak value of  $16 \mu_B^2/\text{eV}/\text{f.u.}$  in the superconducting state at 5 K, which is known from previous work [S1, S3, S4]. In order to account for lattice symmetry, the function  $\text{Im } \chi(\vec{q}, \Omega)$  is cut at the zone center and continued periodically.

Let us now discuss the fitting formula for the normal state data at 70 K. Again, the fitting formula is subdivided into an upper and lower branch. For the lower branch we have

$$\begin{aligned} \text{Im } \chi_\ell(\vec{Q}, \Omega) = & N_0 N_{0\ell} N_{lin}(\Omega) N_\ell(\Omega) N_L(\Omega) \\ & \{ \exp[-4 \ln 2 [((Q_a - Q_{1a})/\sigma_a)^2 + ((Q_b - Q_{1b})/\sigma_b)^2]] \\ & + \exp[-4 \ln 2 [((Q_a - Q_{2a})/\sigma_a)^2 + ((Q_b - Q_{2b})/\sigma_b)^2]] \} \end{aligned} \quad (16)$$

Here, the two Gaussians describe an energy-independent incommensurability with  $\sigma_a = 0.125$  r.l.u.,  $\sigma_b = 0.17$  r.l.u.,  $\mathbf{Q}_1 = (Q_{1a}, Q_{1b}) = (0.575, 0.5)$  r.l.u., and  $\mathbf{Q}_2 = (Q_{2a}, Q_{2b}) = (0.425, 0.5)$  r.l.u. The normalization factors are given by  $N_{0\ell} = 0.001807$ ,

$$N_\ell(\Omega) = 1 - \frac{0.5}{1 + \exp[(\Omega - 29.5)/2]} \quad (17)$$

and

$$N_L(\Omega) = \frac{1}{1 + \exp[(\Omega - 37)/2]}. \quad (18)$$

These factors essentially cut off the lower branch at frequencies above 37 meV and partially below 29.5 meV. The factor

$$N_{lin}(\Omega) = \begin{cases} 1 & \text{for } \Omega \geq 27 \text{ meV} \\ \Omega/27 & \text{for } \Omega < 27 \text{ meV} \end{cases} \quad (19)$$

represents a simple linear decrease below 27 meV consistent with previous work [S5]. For the upper branch we have the same expression as in the superconducting state at 5 K except that

$$N_{dip}(\Omega) = 1 \quad (20)$$

and

$$N_u(\Omega) = 1 - \frac{1.02}{1 + \exp[(\Omega - 37)/2]}. \quad (21)$$

Figure S1 shows the momentum integrated  $\text{Im } \chi(\vec{q}, \Omega)$  in absolute units obtained from the two formulae. The “sum-rule” integral

$$S = \int_0^\infty \frac{d\Omega}{\pi} \left\langle \frac{\text{Im } \chi(Q, \Omega)}{g^2 \mu_B^2} \right\rangle_Q \quad (22)$$

for the two fits gives  $S = 0.071/\text{f.u.}$  for the normal phase ( $T = 70$  K) and  $0.070/\text{f.u.}$  for the superconducting phase ( $T = 5$  K). These numbers are in reasonable agreement with each other.

Figure S2 shows typical measured scans compared with our fit formula convoluted with the instrumental resolution function and demonstrates the good agreement.

In order to check the sensitivity of our results to the high energy part of the magnetic excitation spectrum, we have repeated our calculations with a spectrum cut off at 200 meV.

As a result we found that the coupling constant  $\bar{U}$  had to be increased by 3 percent.  $T_c$  was found to decrease by 1 Kelvin, showing that the details of the high energy part of the spectrum do not affect  $T_c$  very much.

Further on, we have phenomenologically added a normal state  $d$ -wave pseudogap of 30 meV into our calculation and found that  $T_c$  increases by 20 percent, due to the suppression of pairbreaking low-energy magnetic excitations. We conclude that the influence of the pseudogap does not alter our two major findings: the high value of  $T_c$  and the nodal kink generated by the upper branch of the hourglass.

### Fit to fermionic band dispersions

As a starting point for our theoretical calculation we also need the unrenormalized dispersions  $\epsilon_k^{A,B}$  for the bonding (B) and antibonding (A) bands of the two-layer system. In contrast to previous calculations, here we keep the renormalized Fermi surface fixed during the iterative solution of Eqs. (1–3) of the main manuscript, because the Fermi surface is known from the ARPES data. In order to achieve this, we keep the renormalized quantity  $\tilde{\epsilon}_k^{A,B} = \epsilon_k^{A,B} + \text{Re} \xi_{A,B}(k, \omega = 0)$  fixed during the calculation and obtain it from tight-binding fits to the ARPES data of the form

$$\mu_{A,B} - 2t_{A,B}(\cos k_x + \cos k_y) + 4t'_{A,B} \cos k_x \cos k_y - 2t''_{A,B}(\cos 2k_x + \cos 2k_y) \quad (23)$$

with the parameters

$$\begin{aligned} \mu_A &= 556 \text{ meV} & t_A &= 409 \text{ meV} & t'_A &= 150 \text{ meV} & t''_A &= 40 \text{ meV} \\ \mu_B &= 417 \text{ meV} & t_B &= 550 \text{ meV} & t'_B &= 231 \text{ meV} & t''_B &= 67 \text{ meV} \end{aligned}$$

which yield excellent descriptions of the ARPES Fermi surfaces (Fig. 2). These parameters are scaled such that the unrenormalized Fermi velocity at the nodal point in the antibonding band equals  $5 \text{ eV}\text{\AA}$ , as found in *ab-initio* bandstructure calculations [S6].

In order to test the sensitivity of the numerical results to the assumed unrenormalized Fermi velocity, we have repeated the calculations with an unrenormalized Fermi velocity of

4 eVÅ, a value that deviates from the *ab-initio* predictions for  $\text{YBa}_2\text{Cu}_3\text{O}_{6+x}$  but is close to the one found in  $\text{Bi}_2\text{Sr}_2\text{Ca}_1\text{Cu}_2\text{O}_{8+\delta}$  [S7]. In order to reproduce the renormalized Fermi velocity, the coupling constant  $\bar{U}$  has to be reduced from 1.59 to 1.23 eV, and the nodal mass renormalization drops from 3.7 to 3.0. As shown in Fig. S3, the agreement of the numerical and ARPES data for the nodal dispersion at higher energies is worse than that obtained with the more realistic parameters in the main text. Nonetheless, the estimate of the critical temperature for *d*-wave superconductivity remains high. For the INS spectrum at 70 K, we obtain a  $\lambda_d = 1.28$ , corresponding to  $T_c = 140$  K.

Correspondence and requests for materials should be addressed to B.K. (b.keimer@fkf.mpg.de).

## References

- S1. Hayden, S. M., *et al.* The structure of the high-energy spin excitations in a high-transition-temperature superconductor. *Nature* **429**, 531–534 (2004).
- S2. Hinkov, V. *et al.* Spin dynamics in the pseudogap state of a high-temperature superconductor *Nat. Phys.* **3**, 780–785 (2007).
- S3. Bourges, P. *et al.* High-energy spin excitations in  $\text{YBa}_2\text{Cu}_3\text{O}_{6.5}$ . *Phys. Rev. B* **56**, R11439 (1997).
- S4. Fong, H. F. *et al.* Spin susceptibility in underdoped  $\text{YBa}_2\text{Cu}_3\text{O}_{6+x}$ . *Phys. Rev. B* **61**, 14773 (2000).
- S5. Stock, C. *et al.* Dynamic stripes and resonance in the superconducting and normal phases of  $\text{YBa}_2\text{Cu}_3\text{O}_{6.5}$  ortho-II. *Phys. Rev. B* **69**, 014502 (2004).
- S6. Andersen, O. K., Liechtenstein, A. I., Jepsen, O., Paulsen, F. LDA energy bands, low-energy hamiltonians,  $t'$ ,  $t''$ ,  $t_{\perp}(k)$ , and  $J_{\perp}$ . *J. Phys. Chem. Solids* **56**, 1573 (1995).
- S7. Kordyuk, A. A. *et al.* Bare electron dispersion from experiment: Self-consistent self-energy analysis of photoemission data. *et al.*, *Phys. Rev. B* **71**, 214513 (2005).

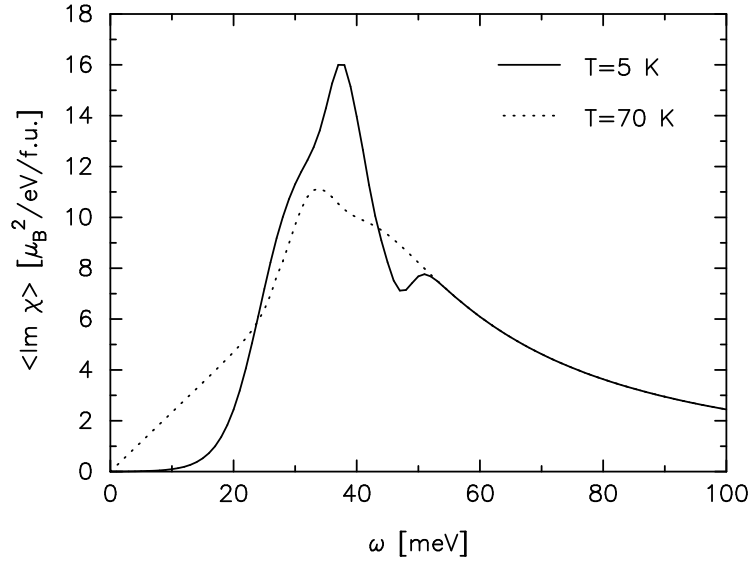


FIG. 1: Momentum-integrated spin excitation spectra at  $T = 5 \text{ K}$  and  $T = 70 \text{ K}$  according to the fitting formulae.

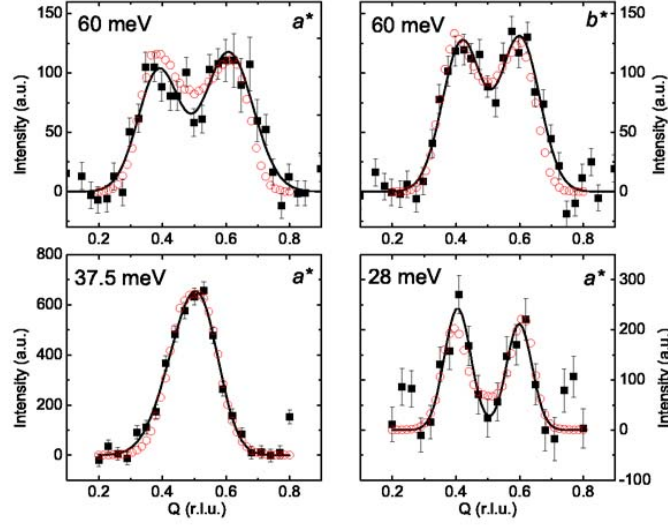


FIG. 2: Comparison of typical constant-energy scans at  $T = 5$  K (black squares) with our fit formula convoluted with the instrumental resolution function (open circles). The black lines are guides to the eye for the measured data points. High- and low-energy scans were measured at different  $k_f$ , thus the intensities are not comparable.

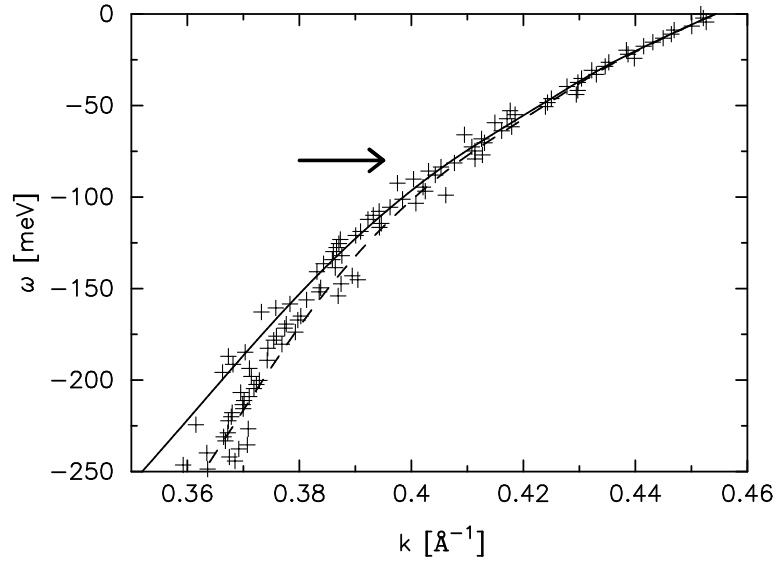


FIG. 3: Comparison of the nodal dispersion measured by ARPES (crosses) and evaluated theoretically for unrenormalized Fermi velocities of  $4 \text{ eV}\text{\AA}$  (solid line) and  $5 \text{ eV}\text{\AA}$  (dashed line).